Canadian Mineralogist
Vol. 17, pp. 679-691 (1979)

MICROSTRUCTURES OF CHRYSOTILE AND ANTIGORITE BY HIGH-RESOLUTION ELECTRON MICROSCOPY

K. YADA

Research Institute for Scientific Measurements, Tohoku University, Sendai, Japan

ABSTRACT

Serpentine minerals are very sensitive to electron-beam irradiation and become amorphous under the intense beam necessary for high-resolution imaging. Image-processing techniques of translational superposition and optical filtering resulted in improved signal-to-noise ratio. The enhanced microstructure images and the electron-diffraction patterns support the following inferences: (a) The β of clinochrysotile measured from the 202 spots is close to the literature value of 93.3°, but fluctuates by $\pm$ 0.5 to 1.0° from fibre to fibre. (b) The resolution of the silicate tetrahedra and brucite octahedra in the unit layers of chrysotile, and of the 180° rotation of alternate layers, provides direct evidence of a structural difference between clino- and orthochrysotile. (c) Of the three proposed models for the antigorite structure (rectified-wave, alternating-wave and zigzag), the alternating-wave structure is valid, even though the arc lengths of successive half-cycles may be unequal, in some cases extremely so. The image of the structure may resemble a rectified-wave or zigzag structure if the specimen is too thick or misoriented. (d) Fault planes (001) in antigorite involve microtwinning. (e) Occasional isolated antigorite areas with $c = 14.6$ Å suggest a two-layer structure. They could, however, be due to radiation damage.

SOMMAIRE

Les minéraux de la famille des serpentines, très sensibles à l'irradiation électronique, s'amorphisent dans le faisceau intense que requiert la formation d'images à haute résolution. Par les techniques de superposition translationnelle et filtrage optique, on améliore le rapport du signal au bruit de fond. Des images ainsi améliorées de la microstructure ainsi que des clichés de diffraction électronique, on tire ces conclusions: (a) L'angle β du clinochrysotile, mesuré sur taches 202, est proche de la valeur connue de 93.3°, mais fluctue de $\pm$ 0.5 à 1.0° d'une fibre à une autre. (b) Les tétraèdres silicatés et octaèdres $Mg(OH)_6$ sont résolus dans la couche unitaire du chrysotile, ainsi que les rotations de 180° entre couches successives, preuve expérimentale directe d'une différence structurale entre clino- et orthochrysotile. (c) Des trois modèles proposés pour la structure de l'antigorite (onde rectifiée, alternative ou en zigzag), c'est le deuxième qui s'applique, bien que les longueurs d'arc de deux demi-cycles successifs soient parfois inégales, même très inégales en certains cas. L'image structurale peut simuler une onde rectifiée ou en zigzag si l'échantillon est trop épais ou désorienté. (d) Des plans de dislocation (001) dans l'antigorite sont associés à un micromaclage. (e) Quelques régions isolées d'antigorite à $c = 14.6$ Å indiqueraient une structure à deux couches, mais il se peut qu'elles proviennent d'un endommagement de l'échantillon par la radiation.

(Traduit par la Rédaction)

INTRODUCTION

High-resolution lattice imaging has made a significant contribution to the structural and chemical study of minerals, as a complementary means to X-ray analysis, but it must be emphasized that this technique has its limitations: many minerals are sensitive to the vacuum environment of the electron microscope and, more seriously, to the electron beam. The latter is particularly true in the case of serpentine.

The fine grain-size of the serpentine minerals chrysotile, lizardite and antigorite makes them suitable for electron microscopy, but little high-resolution work has been done because of their high sensitivity to the electron beam. They easily become amorphous under the intense beam necessary for high-resolution electron microscopy, though antigorite seems to be a little more resistant to the electron beam than chrysotile or lizardite. Accordingly, electron-optics magnification for observation and recording is limited to low levels, and the images are necessarily poor because of noise.

Although the present author has applied the high-resolution lattice-imaging technique to serpentine minerals and has obtained some results that reveal the microstructure (Yada 1967, 1971) and the growth mechanism of chrysotile (Yada & Iishi 1974, 1977), the full potential of recent high-resolution electron microscopy has not yet been reached; possibilities still remain for revealing the structure of the serpentine minerals.

The present author has tried to reduce the radiation damage of serpentine by cooling the specimen and by using a high-voltage microscope, but without satisfactory results. The image-processing technique has therefore been refined to improve the signal-to-noise ratio of the lattice images of serpentine. The main aims of this work are (1) to study the possibility of seeing the atomic arrangement in the serpentine unit-cell directly, (2) to illustrate the structural differences between the polytypes of chrysotile and (3) to discriminate among the three proposed models for the antigorite structure.

According to a recent reappraisal of the serpentine structures by Wicks & Whittaker (1975), clino- and orthochrysotiles with a 5.3 Å fibre axis can be regarded as polytypes. Also, a number of possible values of β exist as a result of different types of stacking, in addition to the usually accepted values of 93.3° for clinochrysotile and 90° for orthochrysotile. It is difficult to prove this clearly by X-ray diffraction, because the sample consists of a large number of fibres, which necessarily gives a kind of mean value of β. In contrast to this, electron microscopy coupled with selected-area electron diffraction may provide clearer evidence because patterns from individual fibres that are sufficiently isolated can be obtained, as well as experimental information about the distribution of β values. However, such isolated fibres are rarely available, because many fibres are mounted in bundles on the grid for electron microscopy.

If the resolution of a lattice image is sufficiently high that some of the 20*l* planes of chrysotile are resolved, the corresponding 20*l* spots can be obtained by optical diffraction for each fibre, even if the fibres are in bundles. Thus, it may be possible to determine the value of β for each fibre. Moreover, it should be possible to make the relative positions of the silicon–oxygen tetrahedra and the magnesium–oxygen octahedra visible by using the image-processing technique, which would then give information about the mode of stacking responsible for the structural features, bearing on the difference between clinochrysotile and orthochrysotile. Thus, a direct demonstration of the structures with alternate layers rotated by 180° was one of the problems expected to be solved in this work.

Parachrysotile, a polymorph of chrysotile with the *b* axis parallel to the cylinder axis, is usually very rare in natural chrysotile, though it very commonly is encountered in synthetic chrysotile. The microstructure of parachrysotile should be studied by high-resolution lattice imaging because little is known about it.

A corrugated structure of antigorite, first proposed by Onsager (1952), has been considered by several workers. Zussman (1954) showed the existence of a curved, corrugated sheet structure by testing trial structures using the optical-transform method, and inferred that a rectified-wave structure was more plausible than the alternating-wave structure. Zussman's rectified-wave model was disproved by the structure refinements of Kunze (1956, 1958); the alternating-wave structure has been accepted, although direct observation of the actual details has not been achieved.

Lattice-imaging studies of antigorite are rare because of its sensitivity to the electron beam, but it should be possible to reveal the corrugated structure if thin samples sectioned perpendicularly to the *b* axis are observed using suitable conditions to minimize beam damage. Results of high-resolution lattice imaging on chrysotile and antigorite, coupled with image processing, are reported here.

Experimental

The instrumental conditions and specimen-preparation techniques employed for electron microscopy are similar to those already reported (Yada 1967, 1971), except that an objective lens with a small-bore polepiece (Yada & Kawakatsu 1976) was used for higher resolution. The angular aperture of the objective was correspondingly increased so that some of the 20*l* reflections in the 2.5–1.8 Å region were resolved.

The direct observation of individual atoms or molecules by high-resolution structure imaging is possible only in a limited set of favorable conditions, because the structure image is very sensitive to many factors reflecting both specimen and instrument (*e.g.*, thickness, orientation, defocusing and lens aberration). Optimum defocus (or Scherzer focus), which is expressed as $\Delta f = \sqrt{C_s\lambda}$ (where C_s is the spherical-aberration coefficient and λ the wavelength of the electron), is about 600 Å on the under-focus side in the present case. A through-focus series of images was usually taken to obtain the optimum focus, although the maximum number of such pictures was limited to two or three because of the beam damage to the specimen.

It is known that optimum specimen-thickness for high-resolution lattice imaging is very small, in the order of 100 Å or less for 100 kV

electrons. The diameter of chrysotile fibres, ranging from 250–500 Å, is much thicker than the optimum, but because of the curved cylindrical form of the fibre the Bragg reflection that contributes to image formation takes place inside a narrow portion of the fibre (Yada & Iishi 1977). Therefore, the effective thickness for lattice imaging is much less than the actual fibre-thickness, which suggests the possibility of obtaining a high-resolution structure image from a rather thick fibre.

Antigorite embedded in methylmethacrylate was sectioned perpendicular to the *b* axis using an MT-1 Porter–Blum ultramicrotome with a diamond knife. The thickness of the sections produced was controlled to between 250–500 Å. Favorably oriented antigorite mounted on a thin carbon film was selected on the fluorescent screen with the aid of an electron-diffraction survey.

Three types of image processing have been proposed: translational superposition (Markham *et al.* 1964), optical noise-filtering (DeRosier & Klug 1972) and computer noise-filtering (Erickson 1974). The translational-superposition technique is limited in that periodicity enhancement is only one dimensional, but since it is the simplest and easiest in actual operation, it was employed for the image processing of antigorite. The procedure is as follows: an appropriately enlarged image of an original negative is multiply exposed, usually 10 times, using stroboscope light on a photographic film moving at a constant speed so as to synchronize the exposure cycle to the periodicity to be enhanced. The signal-to-noise ratio is improved by the factor $\sqrt{n}$, where n is the number of exposures.

The image processing of chrysotile was carried out by the optical noise-filtering technique, which produces a two-dimensional enhancement. A modified optical diffractometer LD–10 by Eiko Engineering Co. was used for the optical filtering. Computer noise-filtering was not tried.

Samples of chrysotile and antigorite studied in this experiment are listed in Table 1.

TABLE 1. LIST OF SPECIMENS STUDIED

Specimen Number	Locality	Description
C - 1	Coalinga, California, USA(1)	Leathery sheet, mainly clinochrysotile sometimes with a helical cylindrical structure
C - 2	Jeffrey Mine, Québec(2)	Mainly clinochrysotile
C - 3 (M 28002)	Havelock Mine, Swaziland (2)	Mainly Povlen-type orthochrysotile
C - 4 (M 31388)	East Broughton, Québec(2)	Mainly Povlen-type clinochrysotile
A - 1	Kyongsangpuk Do, Korea(3)	a = 40 - 60 Å from present work
A - 2 (M 27749)	Zoblitz, Saxony, Germany(2)	a = 34 - 40 Å from present work

(1) From Dr. Mumpton, Union Carbide, USA
(2) From Dr. Wicks, Royal Ontario Museum, Toronto
(3) From Dr. Iishi, Yamaguchi University, Yamaguchi, Japan.

Results

Structure of chrysotile: measurement of β

If an isolated chrysotile fibre is mounted horizontally on the specimen-supporting film, that is, perpendicular to the electron beam, β can be measured directly as one half of the angle subtended by the two 200 spots at the central 000 spot in the electron-diffraction pattern, plus 90°. However, this ideal orientation is rare, and deviations will usually cause some change in the diffraction pattern. In order that the influence of slight tilting of the fibre on the diffraction spots might be checked, a series of single fibres of clinochrysotile, all with regular cylindrical structures (*i.e.*, no helical structures: Whittaker 1955) from Coalinga, California, and Jeffrey mine, Québec (Yada 1971) was examined. Each was tilted by a few degrees, step by step, and the change of the 20*l* spots was observed. As a result, it was found that the diffraction spots on the zero- and first-layer lines remained unchanged in their appearance, but those on the second-layer lines were sensitive to tilting. The 200 spots became more smeared compared to the 202 and $\bar{2}0\bar{2}$ spots. This is shown in Figure 1, where the angular readings of the tilting stage and the angles subtended by the 200 and 202 spots are noted on each picture. For this series, a single fibre whose axis was nearly perpendicular to the axis of tilting was selected so that the increment of the angular readings could be regarded directly as the increment of the tilting angles of the fibre axis. Angles subtended by the 200 and 202 spots correspond to 2β–180° Figure 2 shows the detailed behavior of the angles subtended by the 200 and 202 spots plotted against the tilting angle of the fibre axis from Figure 1. The symmetry of the curves suggests that the position of the stage at approximately –9.5° seems to be the horizontal position of the fibre. The angles subtended by the 200 spots (solid lines) are very sensitive to the slight tilting, but those subtended by the 202 spots (dotted lines) remain nearly unchanged, although slightly different values, of about 0.5°, exist between the angles obtained from opposite second-layer lines.

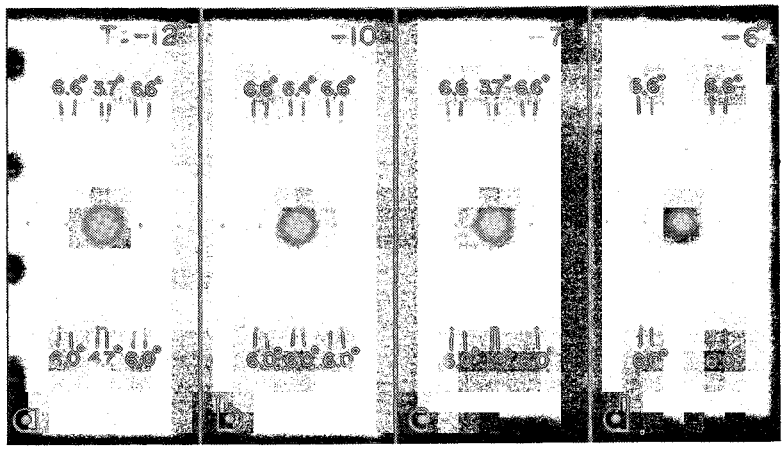

FIG. 1. Changes of the 20*l* spots in the electron-diffraction patterns from a single fibre when the specimen is tilted. T represents angular readings of the tilting stage and the fibre, as the fibre axis is nearly perpendicular to the axis of tilting (C–2). The asymmetric appearance of 20*l* spots on the opposite layer lines is displayed.

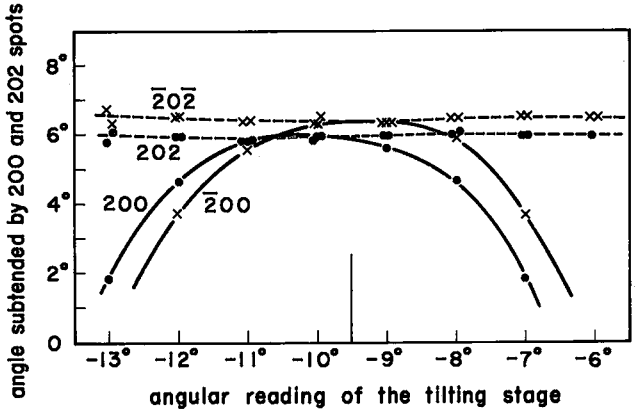

FIG. 2. Variations of the angles subtended by the 200 and 202 spots in the electron-diffraction patterns of Figure 1 against the tilting angles of the stage. The angles subtended by the 200 spots are very sensitive to tilting, whereas those subtended by the 202 spots are insensitive to tilting. The position of –9.5° seems to be the approximate horizontal state of the fibre.

A similar tendency was observed with other clinochrysotile fibres. A β of 93.25° was obtained by averaging the values on the opposite layer lines; this is in good agreement with β previously reported for clinochrysotile (Whittaker 1956). Even if the 200 spots are smeared out or extinct, it is possible to make a rough estimation of β from the 202 spots. The measurements of many fibres show that the angular differences between opposite layer lines vary from fibre to fibre within 0.5° to 1.0°. These angular variations seem greater than the accuracy of the measurements, though their origin is not clear at present. Consequently, there exists a certain variation within $\pm$0.5° in the β values from fibre to fibre.

The β values of 94.1° and 92.5°, suggested by Wicks & Whittaker (1975) for one-layer structures, have not yet been encountered in fibres with a regular cylindrical structure (Whittaker 1955). In fibres with a helical cylindrical structure the measurement of β from the positions of the 200 spots is not possible because the effect of the two factors determining the position of the 200 spots, the helical structure and the tilting of the specimen, cannot be independently assessed. However, the 202 spots appear to be less sensitive to the effects of

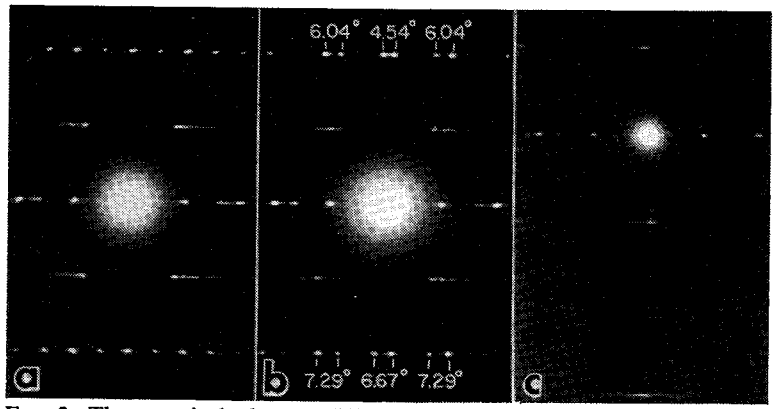

FIG. 3. Three typical electron-diffraction patterns from Povlen-chrysotile (C–2, *M* 28002): (a) orthochrysotile, (b) clinochrysotile and (c) parachrysotile.

the helical structure and give fairly consistent β values of about 93°.

Figure 3 shows typical electron-diffraction patterns of orthochrysotile, clinochrysotile and parachrysotile from cylindrical single fibres in a sample from Havelock mine, Swaziland (*M* 28002). This sample has been considered to be mainly Povlen-type orthochrysotile (Middleton & Whittaker 1976), but actually three kinds of chrysotile occur together. A similar phenomenon was observed in the sample of Povlen-type clinochrysotile (*M* 31388) from East Broughton, Québec (Middleton & Whittaker 1976). The ratio of the components naturally depends on the sample. Electron-diffraction patterns suggest that mixing within one fibre is rarely encountered. In Figure 3(b), the asymmetric appearance of the $20l$ and $-\bar{2}0\bar{l}$ spots, as discussed above, is clearly seen on the opposite layer lines.

Figure 4 is a lattice image of a single fibre corresponding to Figure 3(a), which is typical of orthochrysotile with a regular cylindrical structure. We can see a fringe-profile modulation with a 14.6 Å spacing on the right-hand wall, as indicated by black bars and by the corresponding diffraction spots in its optical-diffraction pattern. A very weak 14.6 Å reflection also occurs on the electron-diffraction pattern. The appearance of this modulation strongly depends on the objective focusing and the thickness of the fibre, and is rarely produced by thin fibres. It is possible to obtain a 14.6 Å reflection on an electron-diffraction pattern by using a very small field-limiting aperture, and by attaining optimum exposure of a fibre that shows the 14.6 Å fringe-profile modulation. The 14.6 Å reflections and fringe-profile modulations have not only been observed from orthochrysotile but also from clinochrysotile, though they are both very rare and faint. However, the nature of the natural chrysotile structure is such that reflections with l odd are not produced. A double-diffraction effect that produces a forbidden reflection is a possible interpretation. In the case of orthochrysotile, for

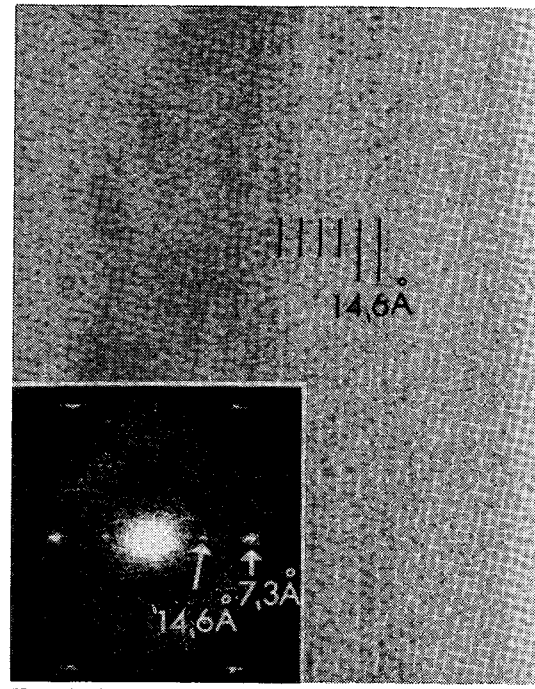

FIG. 4. A lattice image of a single fibre of orthochrysotile and its optical-diffraction pattern, showing 14.6 Å periodicity.

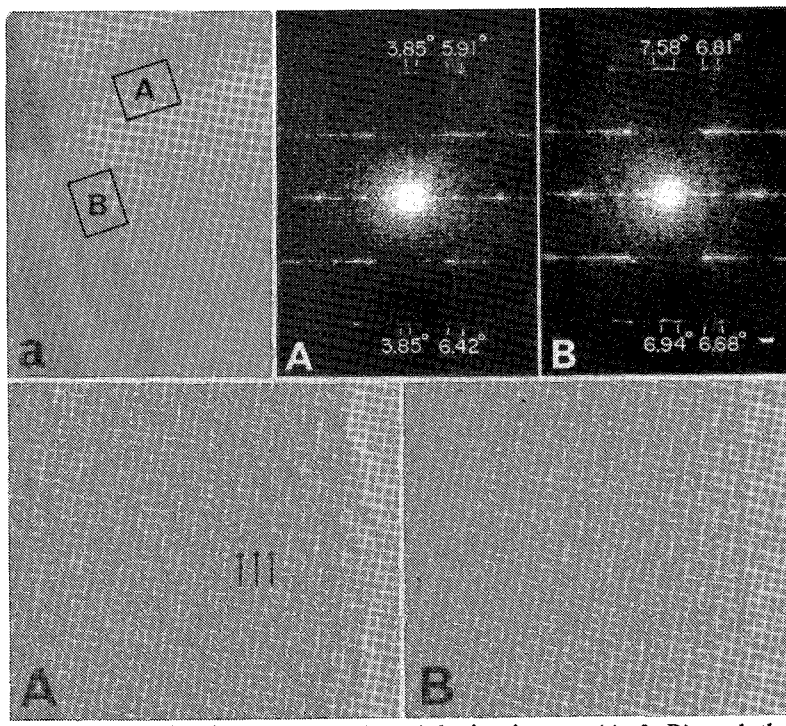

FIG. 5. A lattice image (3), enlarged lattice images (A & B) and the corresponding optical-diffraction patterns (A & B) of clinochrysotile from Coalinga, California (C–1).

instance, the interaction between two primary reflection, such as 200 and $\bar{2}01$, may give rise to the 001 reflection by double diffraction. This is consistent with the fact that the modulation is only observed from rather thick fibres. Whatever the explanation for the 14.6 Å spacing, it does not provide evidence for the two-layer structure of natural chrysotile determined by Whittaker (1953, 1956).

Direct observation of the chrysotile structure

It was found that higher orders of 00*l* and 20*l* reflections, such as 004, 006 and 202, 204 were resolved on optical-diffraction patterns of lattice images of chrysotile. Although image contrast corresponding to these reflections is very faint on the pictures, it can be improved greatly by suppressing the intensity of the 000 reflection through the process of optical filtering.

Figure 5 shows high-resolution images of chrysotile from Coalinga, California, and the corresponding optical-diffraction patterns. Both fibres A and B are clinochrysotile, but A has a regular cylindrical structure and B has a helical structure. The average β values from the 202 and $\bar{2}02$ spots are 93.1° for A and 93.4° for B. The considerably larger angles subtended by the 200 spots in B seem to be due to the helical nature of the structure.

The silicate and "brucite" layers constituting the serpentine structure contain the frameworks of silicon and magnesium cations in them, and their scattering powers for the electron beam are nearly comparable. One third of the 7.3 Å layer is occupied by silicon cations and one third by magnesium cations. The remaining third is not occupied. Therefore, every 7.3 Å fringe should have fine-contrast details consisting of three parts along the *c* direction, under an appropriate focus condition. In Figure 5, the white contrast in every 7.3 Å fringe, indicated by arrows, occupies about one third of the 7.3 Å width, so that these narrow white parts are thought to correspond to the cation-free regions in every chrysotile layer. This contrast relationship may be reversed depending on the focusing condition. Figure 6 shows the processed image of fibre A by optical filtering. As the cation-free regions in every layer look bright in this case, the silicon and magnesium sites show dark contrast. The scattering power of oxygen and hydroxyl is so low that their

contribution to the image contrast is thought to be negligible in a first approximation.

Figure 7 shows high-resolution images of fibres from the Havelock mine (*M* 28002); the optical-diffraction pattern (c) indicates that this fibre is typical orthochrysotile. In the processed image (d), it is evident that one third of every 7.3 Å layer is occupied by a dark fringe representing the cation-free region, so that fringe contrast is reversed from the case in Figure 6; two thirds are occupied by bright fringes representing the sites of the silicon and magnesium cations. Also, two types of layer with different structures are stacked regularly, in contrast to the case of clinochrysotile; therefore, it seems that the 180°-rotated layers of orthochrysotile are directly observed.

These two kinds of processed image were compared with the electron-density maps of clino- and orthochrysotile by Whittaker (1953) (Fig. 8) at the same magnification and with the same sense of contrast. Fairly good agreement can be seen between the maps and the observed structures, though detailed analysis of displacements from ideal positions in the stacking along the *a* and *c* directions is a matter

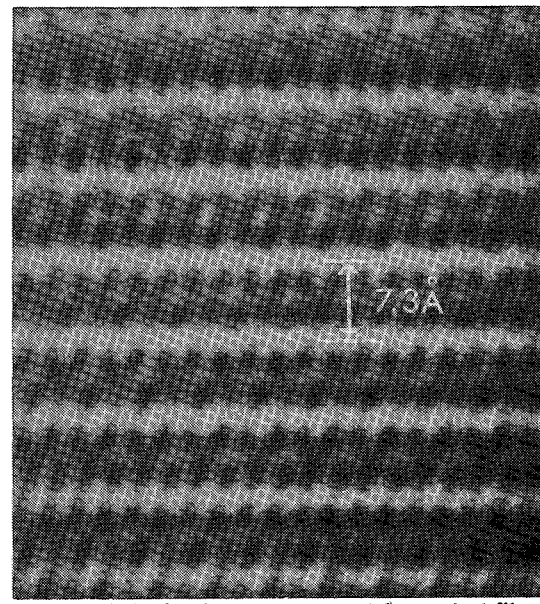

FIG. 6. A lattice image, processed by optical-filtering technique, corresponding to fibre A of Figure 5.

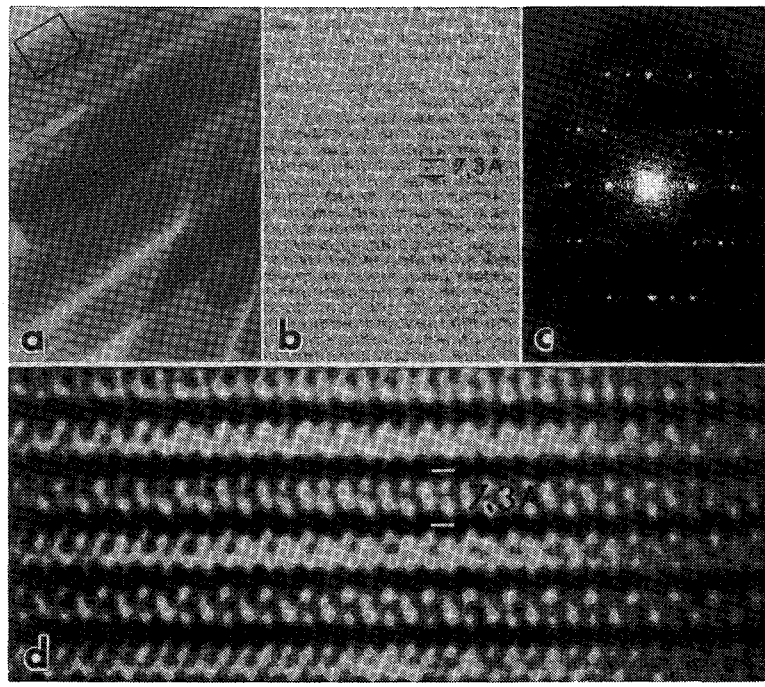

FIG. 7. Lattice images (a and b), the corresponding optical-diffraction pattern (c) and the processed image by optical filtering (d) of orthochrysotile (C–3, *M* 28002).

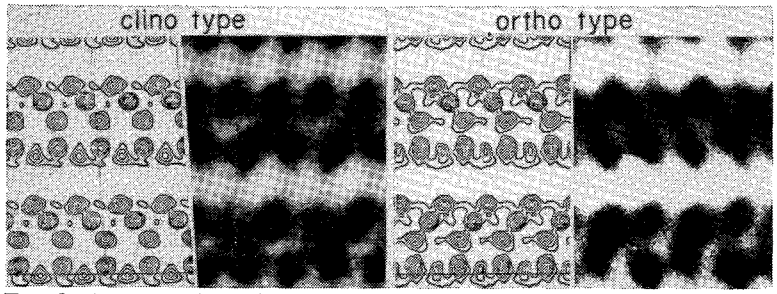

FIG. 8. A comparison between the Fourier projections by Whittaker (1953) and the observed structures of clino- and orthochrysotile.

for future investigation. Results obtained from a similar experiment for parachrysotile will be reported elsewhere.

Microstructure of antigorite

As the main cleavage-plane of antigorite is (001), all previous electron-microscope observations have been made from the direction nearly perpendicular to (001), except for the accidental case of randomly oriented, irregularly fractured fragments. If a specimen lying on (001) is tilted about the *a* axis, 020 spots of the electron-diffraction pattern are split, as seen in (a) to (c) of Figure 9, where tilting angles of the stages are indicated on the electron-diffraction patterns. The 020 (4.6 Å) fringes from such a tilted specimen have a wavy appearance, as shown in Figure 9 (d), where the corresponding optical-diffraction pattern (e) is given; the value of the tilting angle, although large, is unknown. The wavy appearance can be regarded as a reflection of the corrugated structure of antigorite, but direct evidence or detailed information on the inversions in the structure has not been obtained.

From the observation of thin-sectioned anti-

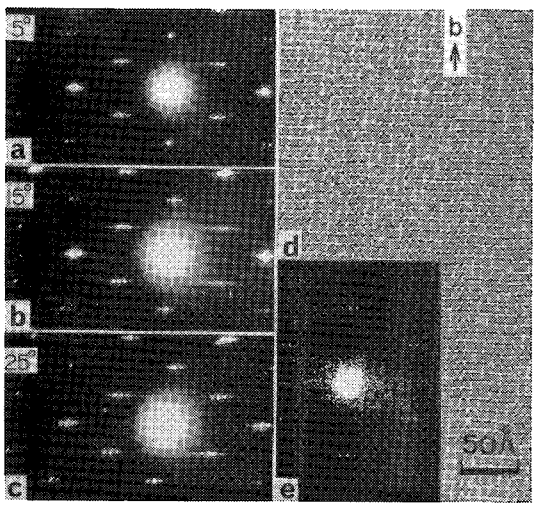

FIG. 9. Changes in the electron-diffraction patterns of antigorite, originally in 001 orientation, tilted around the *a* axis by the angles indicated (a, b and c). The lattice image of the tilted sample (d) with the corresponding optical-diffraction pattern (e) showing a wavy structure perpendicular to the *b* axis (A–1).

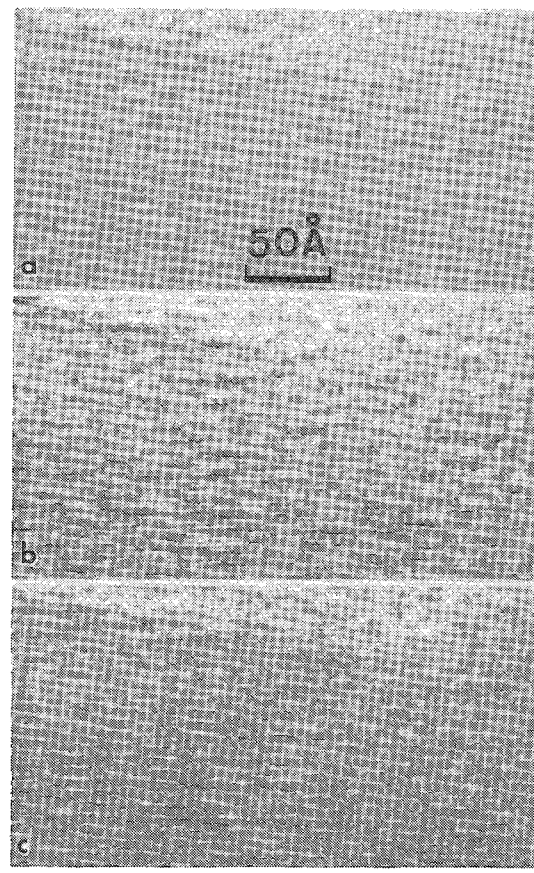

FIG. 10. A through-focus series of lattice images of sectioned antigorite (A–1). The inversion of fringe contrast is seen from (a) to (c).

gorite, single grains, whose dimensions are usually about 0.02–0.2 microns in the *c* direction and up to several microns in the *a* direction, are not always bounded by definite low-index planes such as (001) and (100) but by higher order (*h*0*l*) planes. They sometimes show fault planes such as microtwin planes on (001), as well as extra half-planes due to dislocations.

As mentioned above, the appearance of the lattice image is expected to be very sensitive to specimen orientation and thickness and to the focusing of the objective. Figure 10 shows a through-focal series of a thin section of antigorite from Korea (A-1). This series was taken at rather low magnification with great care to avoid appreciable damage. Slight focal changes from (a) to (c) reverse the fringe contrast from (a) to (b), and again from (b) to (c). Although there are features common to all three images, the details of the fringe structure are quite difficult to distinguish because of the background noise and the damage effects, which are particularly noticeable in (c).

Figure 11 is a result of image processing, by translational superposition, from part of Figure 10(b). The periodicity to be enhanced coincides with the exposure cycle in (b), whereas (a) and (c) correspond to under- and overshift. It is seen that (b) shows a very clear, inversely corrugated structure and a β of approximately 91.5°, which is very close to the value of 91.6° given by Kunze (1956), but the arc lengths of each half-cycle are not equal, as indicated by the black bars.

Figure 12 shows another example of corrugated structure where the half-cycles are nearly equal in length and β is approximately 91.3°. The optical-diffraction pattern (c) is from the processed image of (b).

Thus it can be claimed that the alternating-wave structure has been experimentally proven

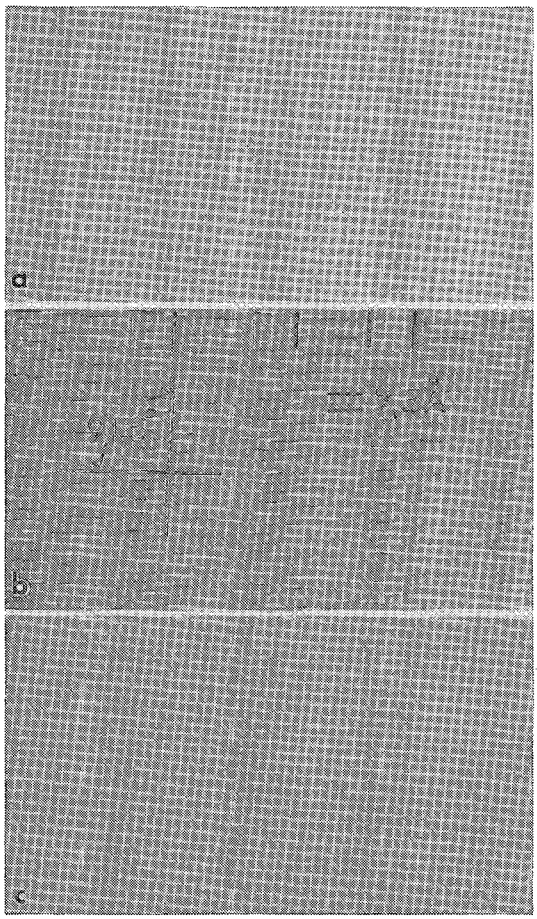

FIG. 11. An example of image processing by translational superposition for part of Figure 10(b). The exposure cycle coincides with the periodicity of the image in (b), but in (a) it is undershifted and in (c) overshifted. An alternating-wave structure is seen in (b), but the arc length of each half-cycle is not equal (A–1).

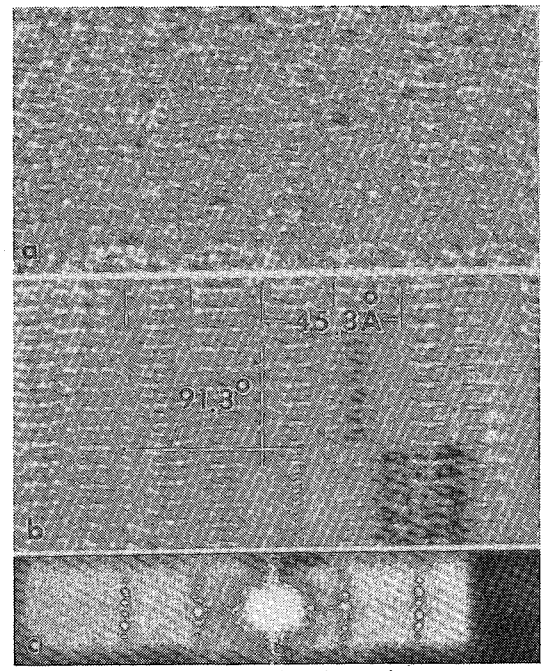

FIG. 12. An example of the alternating-wave structure of antigorite where the arc length of each half-cycle is nearly equal; (a) original image, (b) processed image, (c) optical-diffraction pattern from (b), where the pattern is positioned at right angles with respect to the image (b).

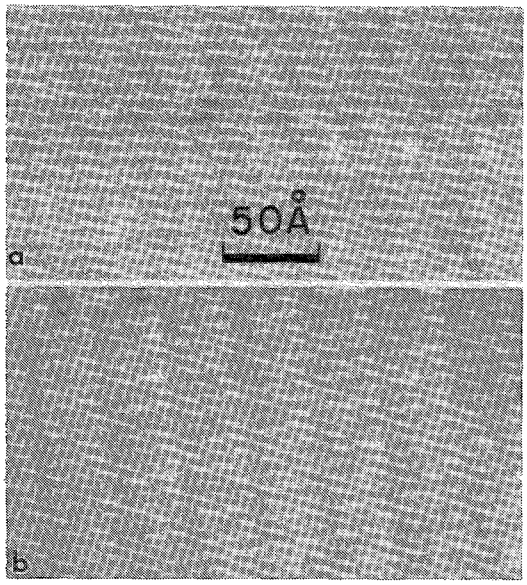

FIG. 13. Images of (a) an apparent rectified-wave structure and (b) an apparent zigzag structure, produced by misoriented alternating-wave structures.

valid, but careful consideration must be given to the possible existence of other structures. Thus, pictures that might suggest other types of structure were looked for. Examples are shown in Figure 13, where (a) resembles the rectified-wave structure and (b) the zigzag structure. After careful consideration, however, it was found that these are not real structures, but effects produced partly by deviation of specimen orientation from the ideal [010] orientation, and partly by too thick a specimen.

If the specimen is very thin, the condition for Bragg diffraction is achieved and the image of the structure is expected to be close to the true structure even in the case of a slight deviation from the ideal orientation. This was proved in an actual case where the crystalline part of the specimen became thinner and thinner due to the electron-beam damage. Although damage to antigorite is serious and generally unfavorable, it always occurs from the outside of the crystal towards the inside, as in the case of chrysotile. Thinning of the crystalline part as well as reduction in its width are thus realized.

Figure 14 shows the damage effect in antigorite, where the effective thickness is greatly reduced from (a) to (d). Figure 15 shows the corresponding structure-images from the framed parts of Figure 14. The inversely corrugated structure is not clear in (a) and (b) but becomes very clear in (c) and (d). In this series a focal effect is involved because the objective focus was changed slightly from (a) to (c). However, it can be proved that the effect of the thickness is much more important than the focal effect if the specimen orientation deviates slightly from the ideal. An example is shown in Figure 16, in which the thickness is increased in a wedge from the upper right to the lower left as indicated by

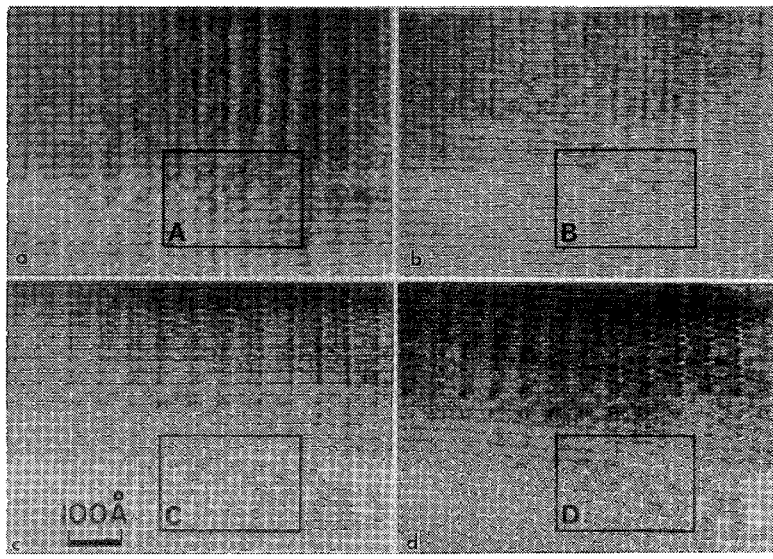

FIG. 14. A series illustrating thinning due to radiation damage (A–1).

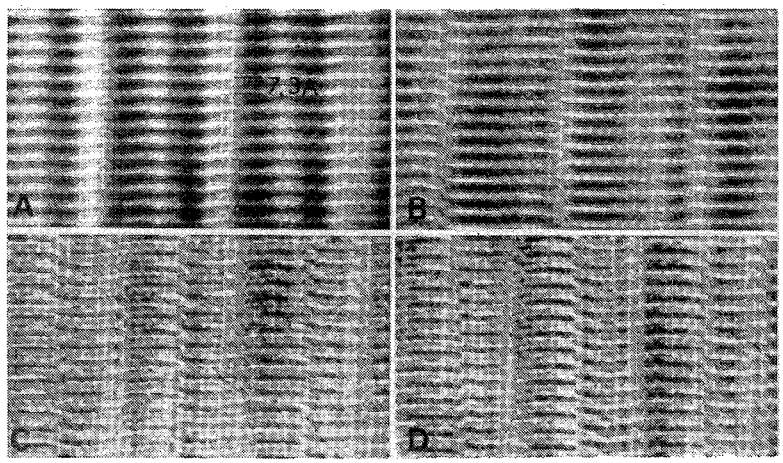

FIG. 15. Images processed by translational superposition corresponding to A to D of Figure 14. The inversely corrugated structure becomes clear with thinning.

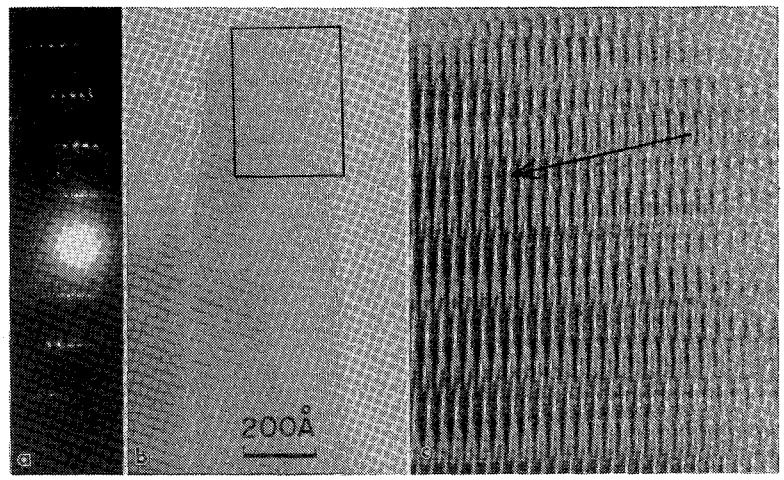

FIG. 16. An illustration of the effect of thickness on the image of the alternating-wave structure. The black arrow indicates the increase in thickness. The inversely corrugated structure is seen in the thin part but not in the thicker part (A–2).

an arrow in the processed image (c). The orientation deviates slightly from the ideal [010], as suggested by the asymmetry of the electron-diffraction pattern (a). In (c) the image of the thinnest part, in the upper right corner, shows the typical inversely corrugated structure, but it seems to change gradually with increasing thickness to an apparent periodically inverted structure.

Areas showing features of a two-layer structure, that is, a repetition of a 14.6 Å periodicity, were rarely found along the [001] direction of the sectioned antigorite, but Figure 17 is an example of a corrugated two-layer structure. Figure 18 is another example of a two-layer structure where A and B were obtained from adjacent but different grains. A and B in the lower images, processed with the repetition of 14.6 Å, show more clearly the two-layer and one-layer character of the structures. In general, the area of the two-layer structure is very localized and seems to become noticeable after irradiation by the electron beam.

CONCLUSIONS

The position of the 200 spots of clinochrysotile on electron-diffraction patterns or op-

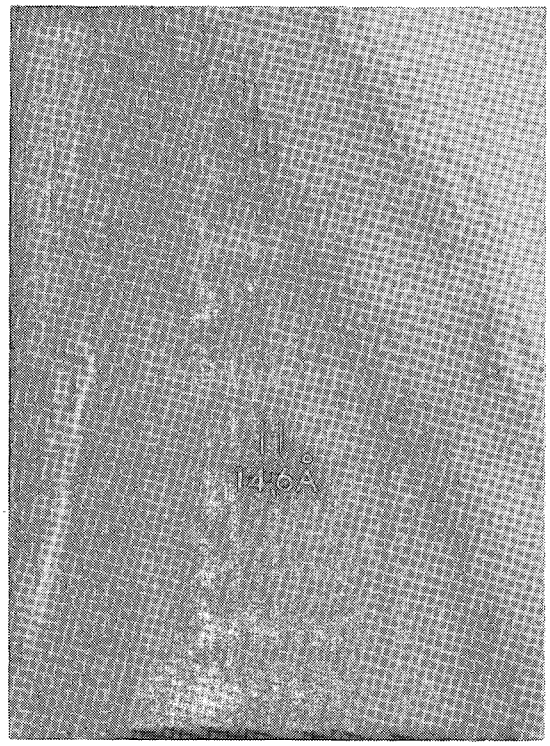

FIG. 17. Two-layer structure of antigorite (A–1).

tical-diffraction patterns of the lattice images is very sensitive to slight tilting of the fibre with respect to the electron beam; thus it is difficult to measure β from the 200 spots. The position of the 202 spots is not greatly affected by slight tilting and gives a more dependable measurement of β (93.3°), similar to the previously determined value. However, it is not possible to determine the β values definitely because of a variation of ± 0.5 to 1.0° between the values obtained on opposite second-layer lines on the same diffraction pattern and from diffraction patterns of different fibres. This asymmetric arrangement of $20l$ and $\bar{2}0\bar{l}$ spots may have been observed before by some workers but there seems to be no report of it. No possible explanation of this phenomenon exists at present. The other possible values of β suggested by Wicks & Whittaker (1975), 94.1° and 92.5° for one-layer structures, have not been demonstrated in this work with fibres having a regular cylindrical structure.

The relative arrangement of silica tetrahedra and brucite octahedra can be revealed by optical filtering of high-resolution structure images in which some $20l$ spots (*e.g.*, 202, 203, 204) in addition to the $00l$ series were resolved. As a result, a two-layer structure with 180° rotation between layers was observed in ortho-

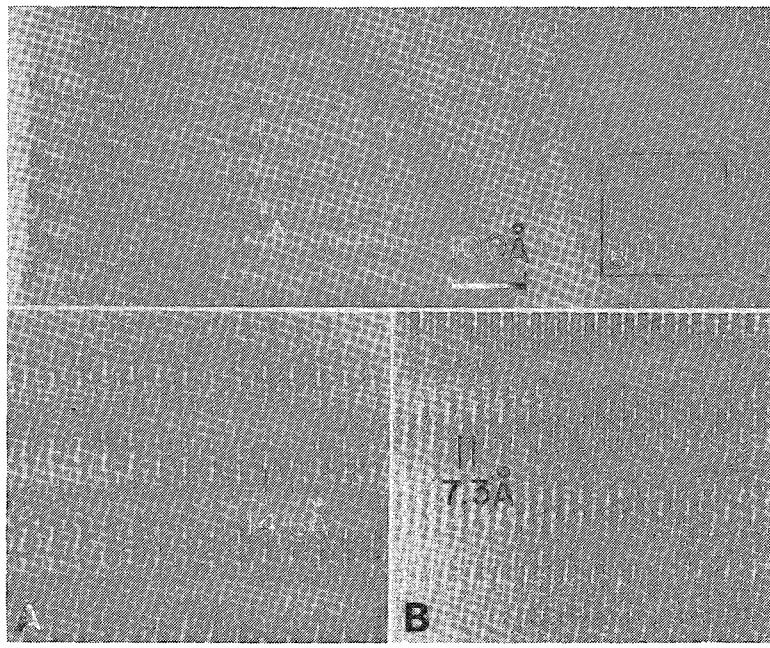

FIG. 18. Two-layer structure of antigorite (A–1). The lower images A and B are from different grains; the images are processed with 14.6 Å repetition.

chrysotile, and a two-layer structure with no rotations in clinochrysotile. Consequently, we can say that the stacking difference between clino- and orthochrysotile as previously predicted has been demonstrated directly. Detailed analysis of the present results will be reported elsewhere. There is a possibility that other stacking varieties may be observed in future by high-resolution structure imaging.

Thin sections of antigorite were observed along the *b* axis by lattice imaging coupled with the image-processing technique, and it was found that the alternating-wave structure of antigorite proposed by Kunze (1956, 1958) was clearly demonstrated in its cross-section, provided that the specimen was thin enough and its orientation was close to the ideal [010] orientation. The radiation damage of the electron beam, which is unfavorable in general, can be utilized for further thinning of sectioned antigorite to produce the correct thickness that will yield images of the true structure. If the specimen orientation deviates considerably from the ideal [010] orientation, images of rectified-wave or zigzag structures are produced, but these do not represent real structures. These images are produced by the alternating-wave structure because of its unfavorable orientation.

By processing the high-resolution image of antigorite by an optical-filtering technique, it is expected that structural details in the antigorite unit-cell will be revealed in the near future, as has been done in the case of chrysotile.

A two-layer structure of antigorite, with 14.6 Å repetition, is rarely encountered but seems to become noticeable after electron-beam irradiation. Whether it is a naturally occurring structure or an artifact produced by radiation damage cannot be determined at this time.

Acknowledgement

The author thanks Mr. S. Takahashi, Mr. K. Shibata and Dr. T. Tanji for their great assistance in the image processing. Thanks are extended to Dr. E. J. W. Whittaker, Reader in Mineralogy, University of Oxford, and Dr. F. J. Wicks, Royal Ontario Museum, Toronto, for their kind provision of serpentine samples and for their discussion and advice on the manuscript.

References

DeRosier, D.J. & Klug, A. (1972): Structure of the tubular variants of the head of bacteriophage T4 (polyheads). *J. Mol. Biol.* **65**, 469-488.

Erickson, H.P. (1974): 2-D image enhancement by optical and computer Fourier techniques. Microtubules and catalase crystals. *Proc. 8th Int. Congr. Electron Micros.* (Canberra) **1**, 310-311.

Kunze, G. (1956): Die gewellte Struktur des Antigorits. I. *Z. Krist.* **108**, 82-107.

——— (1958): Die gewellte Struktur des Antigorits. II. *Z. Krist.* **110**, 282-320.

Markham, R., Hitchborn, J.H., Hills, G.J. & Frey, S. (1964): The anatomy of the tobacco mosaic virus. *Virology* **22**, 342-359.

Middleton, A.P. & Whittaker, E.J.W. (1976): The structure of Povlen-type chrysotile. *Can. Mineral.* **14**, 301-306.

Onsager, L. (1952): Summarized proceedings of a conference on structure of silicate minerals — London, November 1951. *Brit. J. Appl. Phys.* **3**, 277-282.

Whittaker, E.J.W. (1953): The structure of chrysotile. *Acta Cryst.* **6**, 747-748.

——— (1955): A classification of cylindrical lattices. *Acta Cryst.* **8**, 571-574.

——— (1956): The structure of chrysotile. II. Clino-chrysotile. *Acta Cryst.* **9**, 855-862.

Wicks, F.J. & Whittaker, E.J.W. (1975): A reappraisal of the structures of the serpentine minerals. *Can. Mineral.* **13**, 227-243.

Yada, K. (1967): Study of chrysotile asbestos by a high resolution electron microscope. *Acta Cryst.* **23**, 704-707.

——— (1971): Study of microstructure of chrysotile asbestos by high resolution electron microscopy. *Acta Cryst.* **A27**, 659-664.

——— & Iishi, K. (1974): Serpentine minerals hydrothermally synthesized and their microstructures. *J. Crystal Growth* **24/25**, 627-630.

——— & ——— (1977): Growth and microstructure of synthetic chrysotile. *Amer. Mineral.* **62**, 958-965.

——— & Kawakatsu, H. (1976): Magnetic objective lens with small bore. *J. Electron Microsc.* **25**, 1-9.

Zussman, J. (1954): Investigation of the crystal structure of antigorite. *Mineral. Mag.* **30**, 498-512.

Received October 1978, revised manuscript accepted August 1979.